Communication

Effects of Grain Refinement on Tensile Properties and Precipitation Kinetics of Al-Si-Mg Alloys Cast in Sand Molds

FEIYANG CHEN, TAO LU, and YE PAN

Effects of grain refinement on the tensile properties and precipitation kinetics of Al-Si-Mg alloys cast in sand molds by co-alloying of La–B elements were investigated in this work. The kinetics of precipitation after refinement were investigated, including the changes of the precipitation mechanism and decrease of the precipitation activation energy. The reduction of the Avrami exponent indicates the major precipitation mechanism transforms in A359 alloys. Meanwhile, a modified aging process is obtained, which considerably promotes the mechanical properties.

https://doi.org/10.1007/s11663-020-01910-z

Sand mold casting (SMC) is widely used in the production of large-size aluminum alloy castings. However, its lower cooling rate tends to develop coarsening dendrites compared with permanent mold casting.[1] Therefore, many efforts have been made to improve the mechanical properties of aluminum alloys in SMC, but the effects in sand molds are less valid than those in the permanent mold.[2] As we know, the Al-Ti-B refiner is usually used in casting aluminum alloys to refine grains.[3] However, since the formation of Ti-Si compounds consumes the effective content of Ti elements, the Al-5Ti-1B refiner has poor applicability in Al-Si alloys.[4,5] Besides, due to the co-poisoning effect between B and Sr (a commonly used modification element for eutectic Si), the practical application of refiners containing B elements is limited[6–8] LaB_6 has been reported as a potential candidate for an effective refiner of commercial pure aluminum because of its heterogeneous nucleation.[9,10] Pan *et al.* also proposed that co-alloying of La and B elements can greatly improve the refinement of α-Al grains in Sr-modified hypoeutectic aluminum alloys in the permanent mold condition.[11] Hence, the addition of La could avoid the formation of undesired Sr-B compounds during the solidification.[8,12] Since the advantages of La–B co-alloying on grain refinement have been proven in permanent mold casting, it can be predicted that this result is also true in SMC. Another aspect, the refinement of the microstructure, benefits the distribution of the solution elements, such as Mg and/or Cu, during the solidification because of the limitation of chemical segregation.[13] Also, it leads to the formation of more nucleation sites for precipitates.[14] This effect may lead to a different precipitation kinetics of strengthening phases during the heat treatment, especially the age-hardening response.[15–17] Recent articles reported that in permanent molds with high cooling rates, grain refinement altered the precipitation kinetics of the θ′-Al_2Cu phase in Al-Si-Cu-Mg alloys and also improved the mechanical properties after modified heat treatment.[18,19]

Hence, the La–B co-refiner was applied to SMC Al-Si-Mg alloys, and its effects on the properties and aging hardening of Al-Si-Mg alloys are discussed. The variations of microstructures and improvement of tensile strength and elongation of the alloys were investigated in the article. The precipitation kinetics of Mg_2Si and aging treatment of La–B co-refined Al-Si-Mg alloys were analyzed in detail, so better comprehensive properties of Al-Si-Mg alloys were obtained. In general, the La–B co-refiner is valuable for improving the properties of aluminum alloys cast in sand molds.

A356 and A359 alloys were commercial alloys used in SMC and prepared in an electrical resistance furnace. Al-3B and Al-10La master alloys were used to obtain B levels of 0.05 wt pct and La levels of 0.1 wt pct as refinement. It has been proved that the same usage of La–B content can effectively refine the microstructure in the permanent mold casting condition.[20] Al-10Sr was used to obtain an Sr level of 0.03 wt pct as a modification. In addition, the representation of A359 used in this article only indicates that the composition of the sample is close to that of A359 alloys, which are actually cast by gravity casting rather than die casting. The final composition was measured by an optical emission spectrometer (MAXx LMF15), as shown in Table I, which was very close to the nominal one. Due to the limited accuracy of the spectrometer, it should be noted that the actual content of La and B could not be accurately measured and was considered here by the designed addition. The as-cast specimens were cast in sand molds with the size and shape of National Standard GB/T 1173-2013. Then, solution treatment of as-cast specimens was carried out according to GB/T 25745-2010. To investigate the effect of La–B co-refiner

FEIYANG CHEN, TAO LU, and YE PAN are with the Jiangsu Key Laboratory of Advanced Metallic Materials, School of Materials Science and Engineering, Southeast University, Nanjing, 211189 China. Contact e-mail: panye@seu.edu.cn
Manuscript submitted on March 17, 2020.
Article published online July 28, 2020.

Table I. Actual Measured Composition of Each Alloy

Alloys	Condition	Si	Mg	Cu	Sr	Fe	Ti	Al
A356	unrefined	7.0	0.35	0.02	0.03	0.06	0.15	bal.
	co-refined	7.0	0.34	0.02	0.03	0.05	0.14	bal.
A359	unrefined	9.4	0.35	0.03	0.03	0.15	0.00	bal.
	co-refined	9.4	0.35	0.03	0.03	0.13	0.00	bal.

on the precipitation kinetics of Mg_2Si, A356 specimens were aged at 160 °C, 175 °C, 190 °C and 205 °C, respectively, for different times while A359 specimens were immediately aged at the same temperatures and hours. Hardness tests were carried out employing a Brinell hardness tester (220HBS-3000), and each sample was analyzed ten times. The observation of microstructures was carried out using an optical microscope (OM, Olympus BX-60M). The mechanical properties were measured by an electronic universal testing machine (CMT-5105), and three tensile specimens were tested for each alloy.

The microstructures of the un-refined and La–B co-refined A356 alloys are shown in Figure 1, respectively. Both were well modified with the addition of 0.03 wt pct Sr to obtain fibrous eutectic Si phases.

Figure 1(a) shows a typical fine modification of hypoeutectic Al-Si alloys with the typical α-Al dendrites and uniformly distributed eutectic silicon. Figure 1(b) indicates that α-Al dendrites show a slight tendency to be equiaxed after the addition of La–B co-refiner, while Figure 1(c) demonstrates a fully modified eutectic silicon structure in the alloy. The reason can be the presence of the Ti element in the A356 alloy, which consumes the effective content of B leading to weak refinement.[7] Li *et al.*[20] also reported that the Gibbs free energy from the formation of TiB_2 is more negative than that of LaB_6, considering the co-existence of Ti, La and B elements in the melt. Thus, the formation of LaB_6 could be partially transformed to TiB_2, which decreases the efficiency of grain refinement. The microstructures of the un-refined and La–B co-refined A359 alloys are shown in Figure 2. Since the element content of Si is higher than that of A356, eutectic Si occupies a larger area in the metallography. Li *et al.*[20] proved that Fe and Si have no significant impact on refinement. Compared with Figure 1 showing A356, since there is no interference from Ti elements in A359 alloys, more homogeneous distribution and smaller size of equiaxed α-Al dendrites were obtained with 0.1 wt pct La and 0.05 wt pct B addition on the premise of fine modification in Figures 2(b) and (c), consistent with the results of Lu *et al.*[18] Because the α-Al dendrites of A359 show a significant tendency to be equiaxed after refinement, it is no longer possible to distinguish the primary axis dendrites from the secondary dendrites. SDAS values of the specimens could not characterize the microstructure in this work. Hence, a new evaluation method is needed to describe well-equiaxed α-Al dendrites.

The as-cast microstructures for the un-refined specimen and La–B co-refined specimen (both not etched) are obtained in Figure 3, which shows that micro-porosity is hardly observed in either alloy before and after refinement. It can be concluded that the La–B co-refiner has no significant effect on the specimens' porosity.

Furthermore, the grain sizes of both alloys are compared, as shown in Figures 4 and 5. Obviously, finer grains can be obtained after the addition of the La–B co-refiner, and a greater refinement effect is achieved in the A359 than A356 alloy because of the presence of Ti. This is because Ti could consume the content of B, which decreases the number of effective nucleation sites in LaB_6.

The observed precipitation sequence in Al-Si-Mg alloys involves a wide variety of metastable phases, which are different forms of Mg_2Si.[21] Due to the change in micromorphology caused by refinement, it is predictable that the distribution and behavior of the Mg_2Si precipitation phase will be different, resulting in the difference in hardness change in the aging process. Certainly, we can characterize the precipitation characteristics of heat-treated samples by carrying out hardness tests and reveal the changes in precipitation kinetics. The hardness values *vs* aging time curves are presented in Figure 6 for the un-refined and La–B co-refined A356 and A359 alloys aged at 160 °C, 175 °C, 190 °C and 205 °C, respectively.

The hardness of each alloy increases gradually and then decreases after reaching a peak at different temperatures. As the temperature rises from 160 °C to 205 °C, the aging time of peak hardness is gradually reduced from 8 to 9 hours to 3 to 4 hours. This time was further shortened to different degrees after the addition of La–B co-refiner. The curves demonstrate the analogous age-hardening behaviors of A356 and A359 according to the following rules: (1) when the aging temperature is increased, the aging time of peak hardness is advanced; (2) after refinement, the peak hardness values become higher with decreasing aging time; (3) due to the presence of Ti, the microstructure of A356 alloys shows no distinct changes compared with the A359 alloys after La/B addition, which causes limited changes in its precipitation behavior.

Based on the above results, the Johnson–Mehl–Avrami (JMA) equation is employed to analyze the effect of microstructure refinement on the

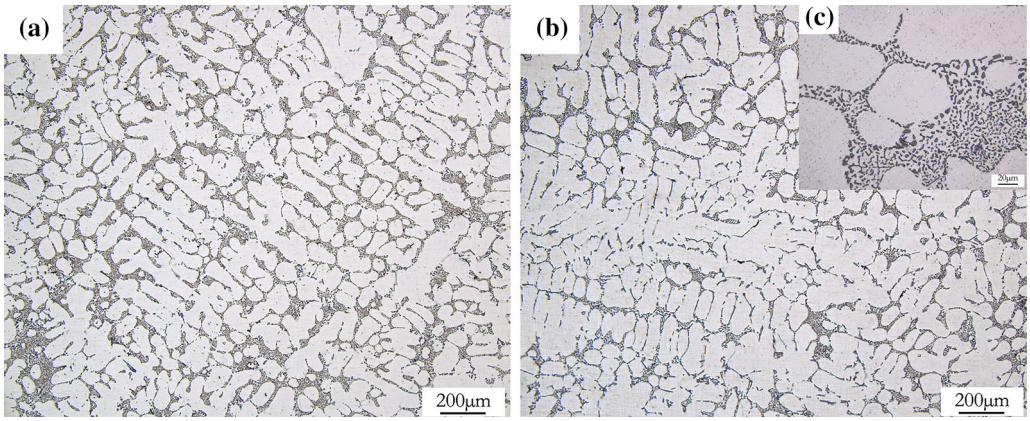

Fig. 1—As-cast microstructures of un-refined (*a*) and La–B co-refined (*b*) A356 (*c*) fully modified eutectic silicon structures of refined alloys.

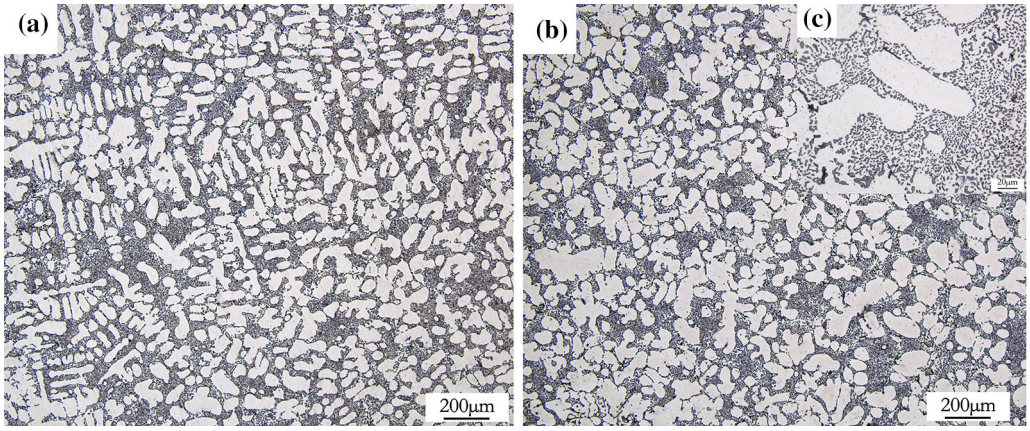

Fig. 2—As-cast microstructures for un-refined (*a*) and La–B co-refined (*b*) A359 (*c*) fully modified eutectic silicon structures of refined alloys.

precipitation kinetics during the aging process. The JMA equation is shown as follows[22]:

$$f = 1 - \exp[-(kt)^n] \quad [1]$$

where f is the transformation fraction, t is the time duration after the beginning of the transformation, k is the rate constant, and n is the Avrami exponent, which is the characteristic coefficient of the transformation process.[23] In this work, Eq. [1] is transformed into the following form:

$$\ln\left(\ln\left(\frac{1}{1-f}\right)\right) = n\ln(k) + n\ln(t) \quad [2]$$

By substituting the experimental data obtained by hardness tests into Eq. [2] to determine the n and k values,[24] the precipitation rate and mechanism can be determined.[25] The value of k can be associated with the thermodynamic Arrhenius equation as follows:

$$k = A\exp\left(-\frac{AE}{RT}\right) \quad [3]$$

where A is a constant; R and T are the gas constant and temperature, respectively. AE stands for the precipitation activation energy. In this work, Eq. [3] is transformed into the following form:

$$\ln(k) = \ln(A) - \frac{AE}{RT} \quad [4]$$

Equation [4] indicates that the values of AE can be obtained by the plots of ln(k) against 1/T.

When applied to study the isothermal precipitation in both aluminum and magnesium alloys,[26] the macroscopic parameter, such as hardness in this work, is frequently used to establish the connections with the microstructure by Eq. [5]:

$$f = \frac{H_t - H_0}{H_{\max} - H_0} \times 100\text{Pct}\ (0 \le t \le t_{\max}) \quad [5]$$

where f is the transformation fraction, H_t is the sample's hardness at time t, and H_0 and $H_{\max}$ are the hardness at the outset and end of the transformation, respectively.

The plots of ln (ln (1/ (1 − *f*))) against ln (*t*) for the un-refined and La–B co-refined A356 and A359 aged at 160 °C, 175 °C, 190 °C and 205 °C are shown in Figures 7 and 8. Evidently, fine linear fitting can be obtained at different temperatures for both alloys showing the

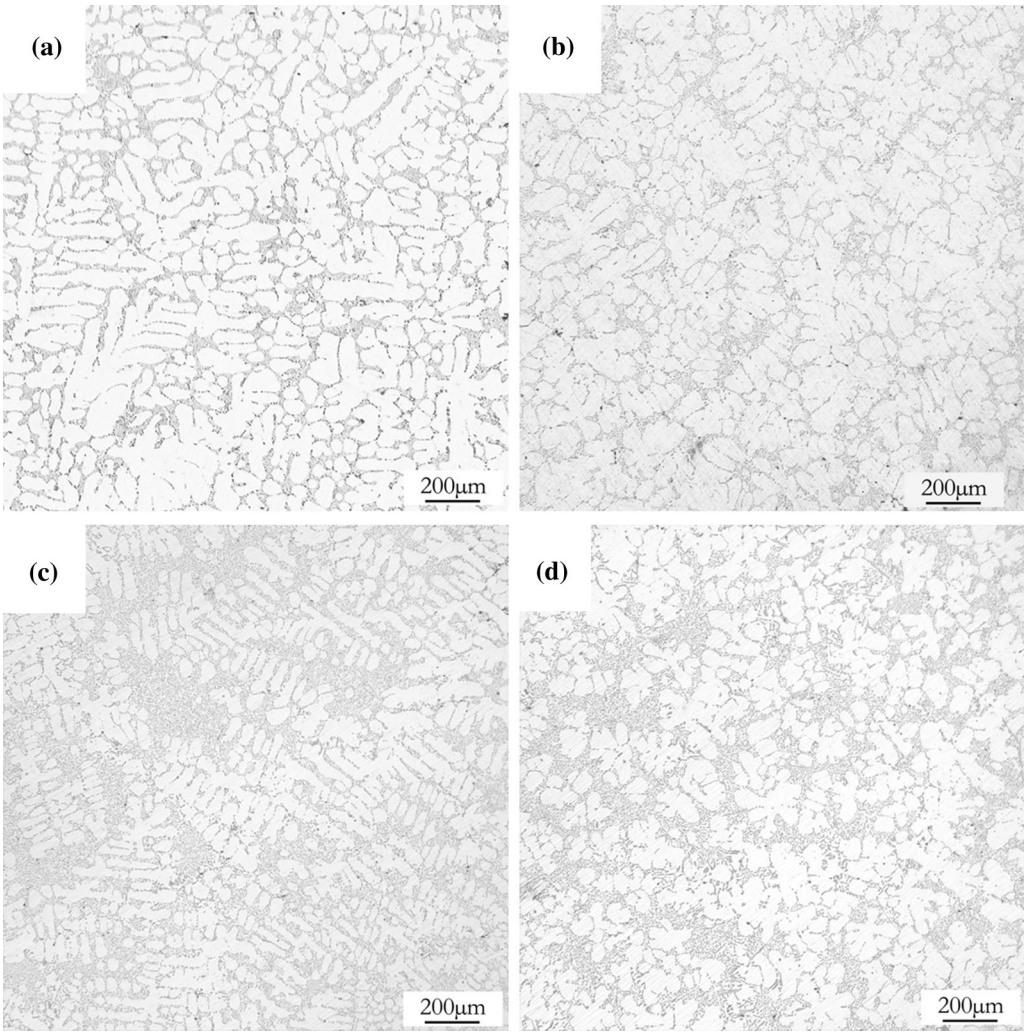

Fig. 3—As-cast microstructures of un-refined (*a*) A356/(*c*) A359 and La–B co-refined (*b*) A356/(*d*) A359 (not etched).

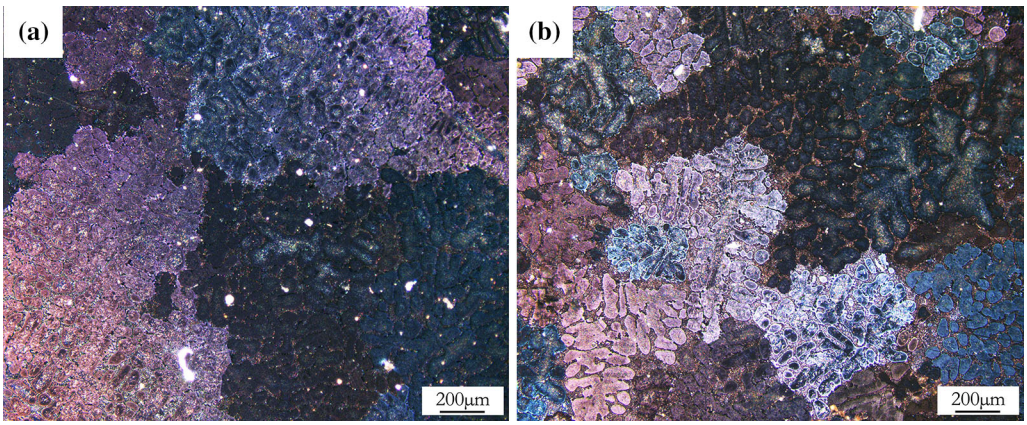

Fig. 4—Grain size of un-refined (*a*) and La–B co-refined (*b*) A356 by polarized light.

precipitation behavior of these alloys illustrated by Eq. [1]. The calculated values of n, $n\ln(k)$ and the correlation coefficient of linear fitting are provided in Table II (A356) and Table III (A359).

The plots of $\ln(k)$ *vs* 1000/RT for these alloys provide the activation energy for precipitation according to Eq. [4], Figures 7(c) and 8(c). In A356 alloys, the values of the activation energy AE are 17.58 kJ/mol for the un-

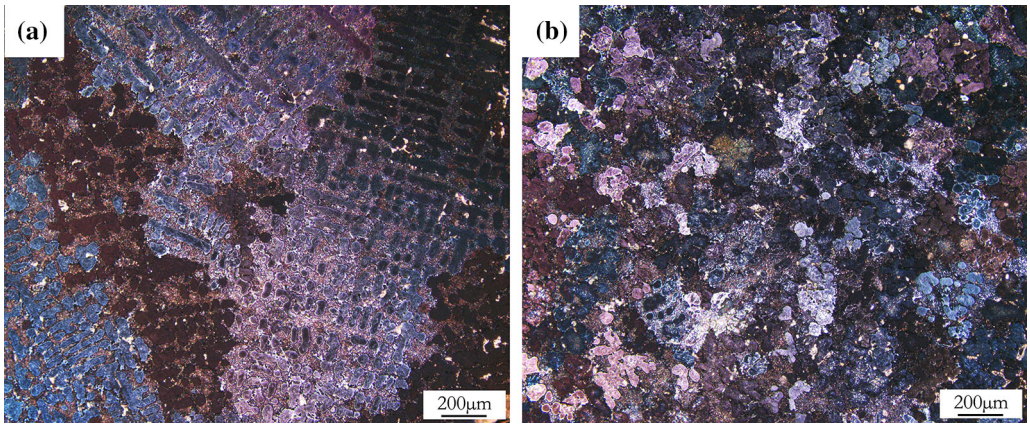

Fig. 5—Grain size of un-refined (*a*) and La–B co-refined (*b*) A359 by polarized light.

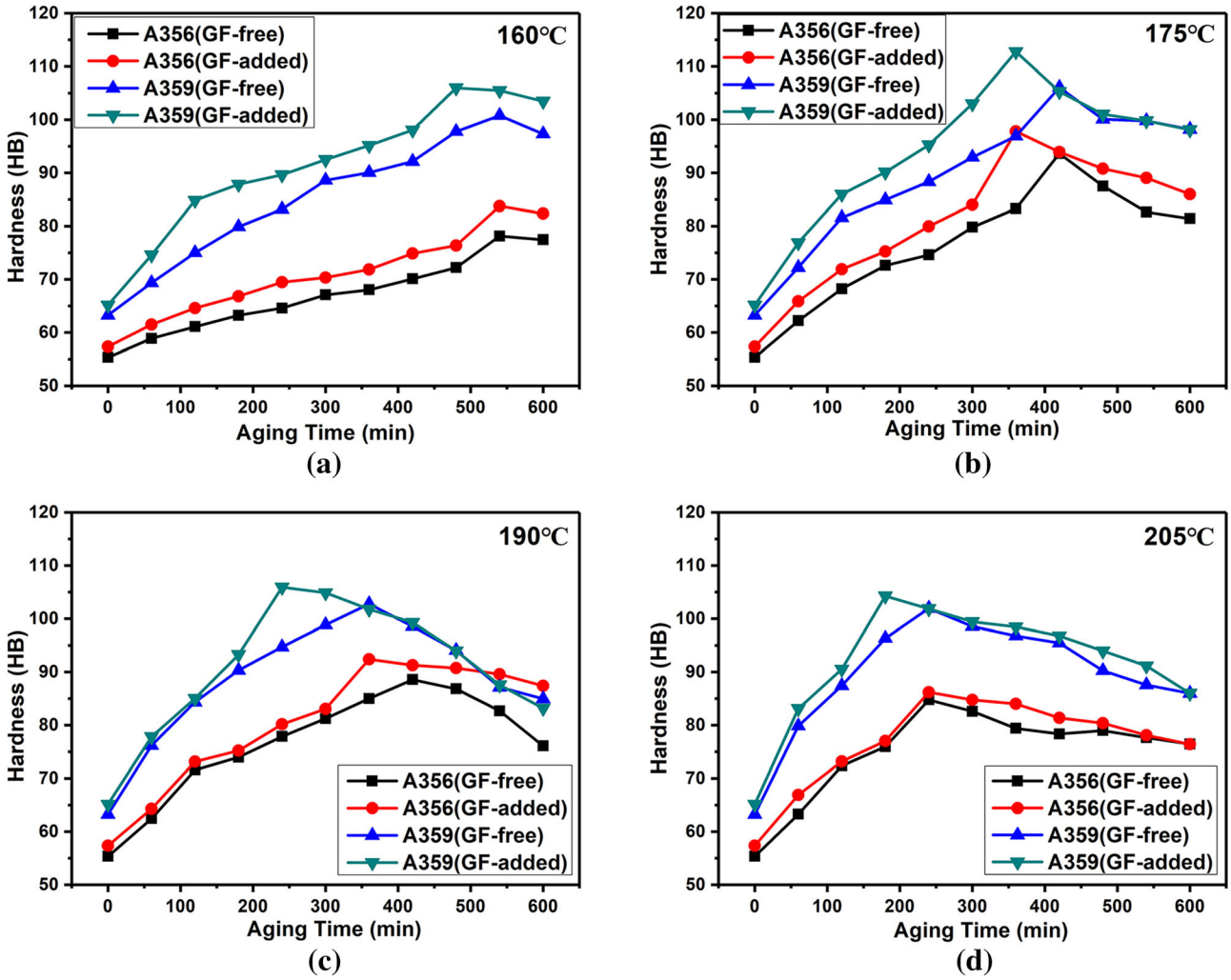

Fig. 6—Hardness curves of un-refined and La–B co-refined A356/A359 aged at 160°C (*a*), 175 °C (*b*), 190 °C (*c*) and 205 °C (*d*).

refined alloy and 15.93 kJ/mol for the La–B co-refined alloy. With the addition of La–B co-refinement, the values of n remain at around 2.4 without a significant decrease, which indicates that precipitation keeps a constant nucleation rate with the diffusion-controlled mechanism.[25] Because the microstructure of A356 alloys does not change significantly, the precipitation mechanism can be considered to have no notable difference; thus, the precipitation rate merely has a finite reduction. However, in A359 alloys, the values of the

Table II. Values of n and $n\ln(k)$ Obtained from Eq. JMA in A356

	Un-Refined				La–B Co-Refined			
	T (°C)				T (°C)			
A356	160	175	190	205	160	175	190	205
n	2.24	2.34	2.65	2.88	2.16	2.07	2.48	2.21
$n\ln(k)$	− 5.86	− 5.79	− 6.09	− 6.23	− 5.64	− 5.12	− 5.85	− 4.84
R^2	0.98	0.99	0.97	0.96	0.99	0.99	0.97	0.99
AE/kJ	17.58				15.93			

Table III. Values of n and $n\ln(k)$ Obtained from Eq. JMA in A359

	Un-refined				La–B Co-refined			
	T (°C)				T (°C)			
A359	160	175	190	205	160	175	190	205
n	2.72	2.28	2.46	2.51	1.98	2.30	2.36	1.97
$n\ln(k)$	− 6.63	− 5.46	− 5.34	− 5.10	− 4.73	− 5.38	− 5.21	− 4.13
R^2	0.97	0.98	0.99	0.92	0.96	0.97	0.96	0.99
AE/kJ	16.58				11.56			

activation energy AE are found to be 16.58 kJ/mol for the un-refined alloy and 11.56 kJ/mol for La–B co-refined alloy, respectively. Meanwhile, the values of n decrease from 2.5 to 2.1 after refinement, which shows that the precipitation mechanism has changed. The precipitation mechanism represented by different n values is shown in Table IV.[25]

The reduction of n indicates the major precipitation mechanism of transforming from the diffusion-controlled one in A356 alloys to a combination of the grain-boundary precipitation and diffusion mechanism in A359 alloys. This is consistent with an elevation of the grain boundary density of A359 alloys due to the more finely equiaxed grain character induced by the co-refinement effect of La and B elements. Moreover, the nucleation of Mg_2Si precipitation during age hardening occurs on the grain boundaries and keeps a constant nucleation rate with diffusion-controlled in the meantime, rather than merely being controlled by diffusion. Without the influence of the Ti element, the well-refined microstructure of A359 alloys cast in sand molds leads to the reduction of the precipitation activation energy and homogenizes the distribution of solution elements, which speeds up the hardening response, as shown in Figure 6.

This research on precipitation kinetics shows clearly that the co-refinement of La–B alters the precipitation behavior, which will leads to the a change of optimized solid solution and aging parameters. According to these results, the solid solution and aging process can be improved to obtain good comprehensive mechanical properties. The heat treatment parameters of each sample are listed in Table V, and the mechanical properties are also evaluated in Tables VI and VII, demonstrating the ultimate tensile strength (R_m), elongation (A) and quality index (Q) of the SMC A356 and A359 alloys in different conditions. Q is an indicator that comprehensively measures strength and plasticity, and its expression is given in Eq. [6].

$$Q = R_m + k\log(A)(MPa) \quad [6]$$

where k is a material constant, which is 150 in this work.[27] In the as-cast condition, there is no significant difference of R_m in either the A356 or A359 alloy, while A is effectively improved by refinement from 3.4 to 6.4 pct in A359 alloys. Similar results appear for the condition of the regular T6 condition. In the modified T6 condition shown in Table V, R_m and A both are remarkably improved, which increases the quality index of A356 alloys from 334.1 to 353.9 MPa, and the Q of A359 alloys increases from 338.8 to 376.6 MPa, respectively. Clearly, La–B co-refinement can achieve a good combination of strength and plasticity of SMC Al-Mg-Si alloys. The more finely equiaxed grain induced by the co-refinement effect of La and B elements could lead to an elevation of grain-boundary density and more nucleation sites for precipitates. Hence, the heat treatment process could be modified to improve the mechanical properties of the alloys because of the changes in precipitation behavior.

In this work, the influences of grain refinement on the tensile properties and precipitation kinetics of Al-Si-Mg alloys cast in sand molds were investigated. Considering the presence or absence of Ti elements, the La–B co-refinement process shows different effects on the microstructure and precipitation kinetics in the alloys, which lead to changes of the properties including strength and plasticity. The following conclusions can be drawn:

A. La–B co-refinement can effectively produce a fine microstructure and make α-Al dendrites equiaxed in Al-Mg-Si alloys under sand mold conditions. Thus,

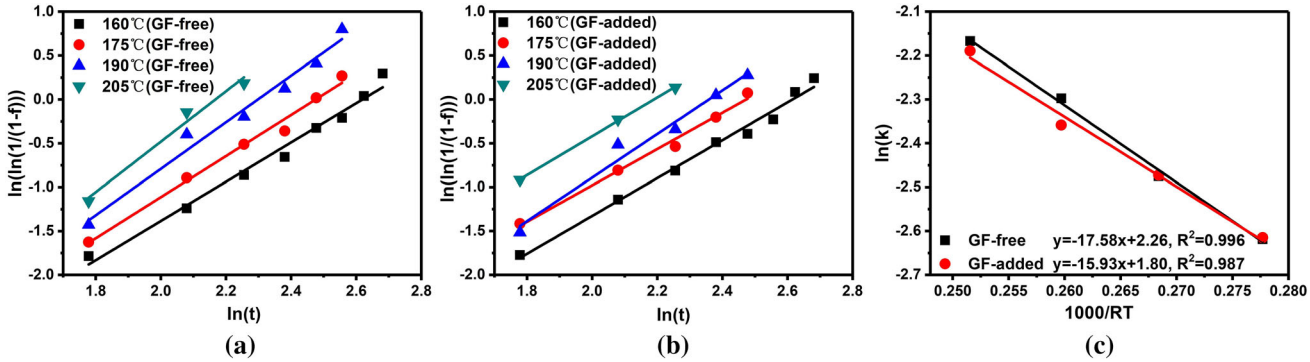

Fig. 7—Curve fit plots of Eq. [2] used to obtain the Avrami exponent n (*a*, *b*) and straight lines relating ln (k) and 1000/RT for un-refined and La–B co-refined A356 (*c*).

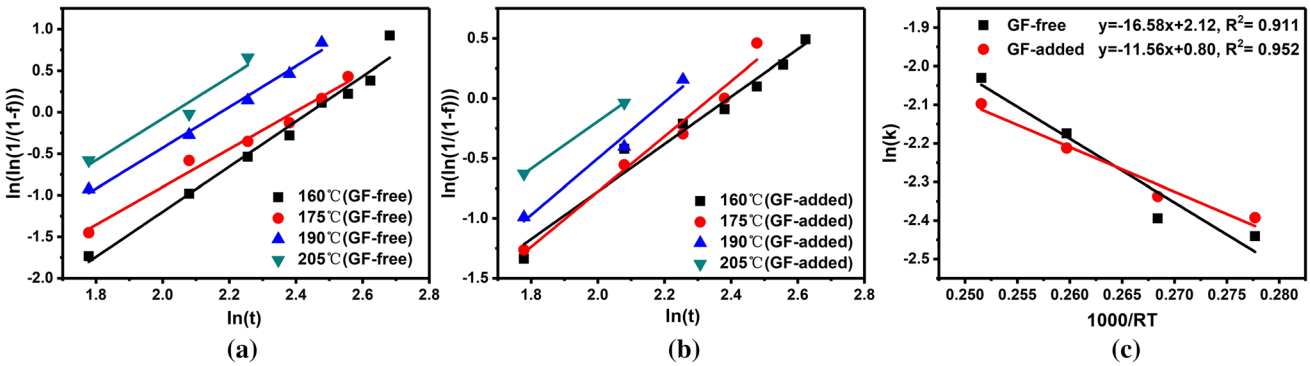

Fig. 8—Curve fit plots of Eq. JMA used to obtain the Avrami exponent n (*a*, *b*) and straight lines relating ln (k) and 1000/RT for un-refined and La–B co-refined A359 (*c*).

Table IV. Precipitation Mechanism Represented by Different *n* Values

Avrami Exponent n	Corresponding Mechanism
4	constant nucleation rate
3~4	decreasing nucleation rate
2.5	constant nucleation rate with diffusion-controlled growth
1	nucleation on grain boundaries
2/3	nucleation on dislocation

Table V. Parameters of Heat Treatment of Each Sample

	Heat Treatment	Solution	Aging
A356	regular T6	530 °C/5 hours	20 °C/12 h + 175 °C/4 hours
	modified T6	535 °C/5 hours	20 °C/12h + 175 °C/6 hours
A359	regular T6	535 °C/6 hours	175 °C/10 hours
	modified T6	535 °C/5 hours	175 °C/6 hours

Table VI. Tensile Properties of Sand Mold Casting A356 Alloys Under Different Conditions

	Condition	R_m (MPa)	A (Pct)	Q (MPa)
As-cast	unrefined	145.5	6.1	263.3
	La–B co-refined	145.9	5.7	259.3
Regular T6	Unrefined	253.0	4.4	349.5
	La–B co-refined	259.4	3.9	348.1
Modified T6	unrefined	239.1	4.3	334.1
	La–B co-refined	254.5	4.6	353.9

Table VII. Tensile Properties of Sand Mold Casting A359 Alloys Under Different Conditions

	Condition	R_m (MPa)	A (Pct)	Q (MPa)
As-Cast	unrefined	154.4	3.4	234.1
	La–B co-refined	151.2	6.4	272.1
Regular T6	unrefined	297.6	1.4	319.5
	La–B co-refined	307.3	1.7	341.9
Modified T6	unrefined	261.0	3.3	338.8
	La–B co-refined	278.6	4.5	376.6

this refining technique is more efficiently applicable to Al-Si-Mg alloys without the Ti element.

B. The calculated Avrami exponent n decreases from 2.5 to 2.1, which demonstrates the major precipitation mechanism transforms from the diffusion-controlled one in the A356 alloy to a combination of grain-boundary precipitation and diffusion mechanism in the A359 alloy. Also, the activation energy of the precipitation decreases from 16.6 kJ/mol in unrefined A359 alloys to 11.6 kJ/mol in refined A359 alloys. All of these are related to the microstructure refinement including small grain and equiaxed α-Al phase.

C. Comprehensive mechanical properties of the Al-Mg-Si alloys cast in sand molds can be effectively improved by microstructure refinement and modified heat treatment. The quality index Q of A356 alloys increases from 334.1 to 353.9 MPa, and that of the A359 alloy increases from 338.8 to 376.6 MPa, respectively. This result shows the new refinement process can shorten the solid-solution and aging process of castings while enhancing strength. It is believed to also reduce the total cost of casting manufacturing.

The authors appreciate the support from Jiangsu Key Laboratory for Advanced Metallic Materials (No. BM2007204).

REFERENCES

1. C.H. Caceres, C.J. Davidson, J.R. Griffiths, and C.L. Newton: *Mater. Sci. Eng. A-Struct. Mater. Prop. Microstruct. Process.*, 2002, vol. 325, pp. 344–55.
2. J.G. Wang, H.Q. Lin, Y.Q. Li, and Q.C. Jiang: *J. Alloys Compd.*, 2008, vol. 457, pp. 251–58.
3. A.L. Greer, A.M. Bunn, A. Tronche, P.V. Evans, and D.J. Bristow: *Acta Mater.*, 2000, vol. 48, pp. 2823–35.
4. Y. Birol: *J. Alloys Compd.*, 2009, vol. 486, pp. 219–22.
5. D. Qiu, J.A. Taylor, M.X. Zhang, and P.M. Kelly: *Acta Mater.*, 2007, vol. 55, pp. 1447–56.
6. T.M. Wang, H.W. Fu, Z.N. Chen, J. Xu, J. Zhu, F. Cao, and T.J. Li: *J. Alloys Compd.*, 2012, vol. 511, pp. 45–49.
7. Y. Birol: *J. Alloys Compd.*, 2012, vol. 513, pp. 150–53.
8. H.C. Liao and G.X. Sun: *Scr. Mater.*, 2003, vol. 48, pp. 1035–39.
9. P.T. Li, C. Li, J.F. Nie, J. Ouyang, and X.F. Liu: *Crystengcomm*, 2013, vol. 15, pp. 411–20.
10. P.T. Li, W.J. Tian, D. Wang, and X.F. Liu: *J. Rare Earths*, 2012, vol. 30, pp. 1172–76.
11. Y. Chen, Y. Pan, T. Lu, S.W. Tao, and J.L. Wu: *Mater. Design.*, 2014, vol. 64, pp. 423–26.
12. E. Samuel, B. Golbahar, A.M. Samuel, H.W. Doty, S. Valtierra, and F.H. Samuel: *Mater. Design*, 2014, vol. 56, pp. 468–79.
13. X.Q. Li, R.P. Jiang, Z.H. Li, L.H. Zhang and X. Zhang, In *Advances In Materials Manufacturing Science And Technology Xiv*, ed. T. Huang, D. Zhang, B. Lin, A.P. Xu, Y.L. Tian and W. Gao (2012), pp 383-88.
14. Z. Rong-da, Z.H.U. Jing-chuan, J. Cheng-wen and L.A.I. Zhong-hong, *Heat Treatment of Metals* 2009, vol. 34, pp. 27-30.
15. J. Buha: *Acta Mater.*, 2008, vol. 56, pp. 3533–42.
16. S. Costa, H. Puga, J. Barbosa, and A.M.P. Pinto: *Mater. Design*, 2012, vol. 42, pp. 347–52.
17. A. Deschamps, F. De Geuser, Z. Horita, S. Lee, and G. Renou: *Acta Mater.*, 2014, vol. 66, pp. 105–17.
18. T. Lu, S. Tao, Y. Chen, Y. Pan, and J. Pi: *Materialwissenschaft Und Werkstofftechnik*, 2017, vol. 48, pp. 101–05.
19. L. Tao, W. Ji-li, Y. Pan, S.-w. Tao, and Yu. Chen: *China Foundry*, 2015, vol. 12, pp. 111–17.
20. C.L. Li, Y. Pan, T. Lu, L.J. Jing, and J.H. Pi: *Met. Mater.-Int.*, 2018, vol. 24, pp. 1133–42.
21. C. Ravi and C. Wolverton: *Acta Mater.*, 2004, vol. 52, pp. 4213–27.
22. J. Malek: *Thermochimica Acta*, 1995, vol. 267, pp. 61–73.
23. M.J. Starink: *J. Mater. Sci.*, 1997, vol. 32, pp. 4061–70.
24. B. Amir Esgandari, H. Mehrjoo, B. Nami and S.M. Miresmaeili, *Mater. Sci. Eng. A-Struct. Mater. Prop. Microstruct. Process.* 2011, vol. 528, pp. 5018-24.
25. K.A. Jackson: *Mater. Today*, 2004, vol. 7, p. 63.
26. A.T. Adorno, R.A.G. Silva, and T.B. Neves: *Mater. Sci. Eng. A-Struct. Mater. Prop. Microstruct. Process.*, 2006, vol. 441, pp. 259–65.
27. M. Tiryakioglu, J. Campbell, and N.D. Alexopoulos: *Metall. Mater. Trans B-Process Metall Mater. Process. Sci.*, 2009, vol. 40, pp. 802–11.